Diagenesis of the Amposta offshore oil reservoir (Amposta Marino C2 well, Lower Cretaceous, Valencia Trough, Spain)

E. PLAYÀ[1], A. TRAVÉ[1], M. A. CAJA[2], R. SALAS[1] AND J. D. MARTÍN-MARTÍN[1]

[1]*Departament de Geoquímica, Petrologia i Prospecció Geològica, Facultat de Geologia, Universitat de Barcelona, C/Martí i Franquès s/n, Barcelona, Spain;* [2]*Departamento de Petrología y Geoquímica, Facultad de Ciencias Geológicas, Universidad Complutense de Madrid, Avda. Jose Antonio Novais, Madrid, Spain*

ABSTRACT

Samples from the Amposta Marino C2 well (Amposta oil field) have been investigated in order to understand the origin of fractures and porosity and to reconstruct the fluid flow history of the basin prior, during and after oil migration. Three main types of fracture systems and four types of calcite cements have been identified. Fracture types A and B are totally filled by calcite cement 1 (CC1) and 2 (CC2), respectively; fracture type A corresponds to pre-Alpine structures, while type B is attributed to fractures developed during the Alpine compression (late Eocene-early Oligocene). The oxygen, carbon and strontium isotope compositions of CC2 are close to those of the host-rock, suggesting a high degree of fluid-rock interaction, and therefore a relatively closed palaeohydrogeological system. Fracture type C, developed during the Neogene extension and enlarged by subaerial exposure, tend to be filled with reddish (CS3r) and greenish (CS3g) microspar calcite sediment and blocky calcite cement type 4 (CC4), and postdated by kaolinite, pyrite, barite and oil. The CS3 generation records lower oxygen and carbon isotopic compositions and higher $^{87}Sr/^{86}Sr$ ratios than the host-limestones. These CS3 karstic infillings recrystallized early within evolved-meteoric waters having very little interaction with the host-rock. Blocky calcite cement type 4 (CC4 generation) has the lowest oxygen isotope ratio and the most radiogenic $^{87}Sr/^{86}Sr$ values, indicating low fluid-rock interaction. The increasingly open palaeohydrogeological system was dominated by migration of hot brines with elevated oxygen isotope ratios into the buried karstic system. The main oil emplacement in the Amposta reservoir occurred after the CC4 event, closely related to the Neogene extensional fractures. Corrosion of CC4 (blocky calcite cement type 4) occurred prior to (or during) petroleum charge, possibly related to kaolinite precipitation from relatively acidic fluids. Barite and pyrite precipitation occurred after this corrosion. The sulphur source associated with the late precipitation of pyrite was likely related to isotopically light sulphur expelled, e.g. as sulphide, from the petroleum source rock (Ascla Fm).

Key words: limestones, calcite cements, fracture porosity, isotopes, Valencia Trough

Received 29 June 2009; accepted 20 October 2009

Corresponding author: E. Playà, Departament de Geoquímica, Petrologia i Prospecció Geològica, Facultat de Geologia, Universitat de Barcelona, C/Martí i Franquès, s/n, 08028 Barcelona, Spain.
Email: eplaya@ub.edu. Tel: 34 3 4021401. Fax: 34 3 4021340.

Geofluids (2010) **10**, 314–333

INTRODUCTION

The Valencia Trough is a Neogene oil-producing basin where accumulations are in Mesozoic and Neogene rocks. Main reservoir rocks are fractured and karstified Jurassic and Lower Cretaceous limestones located at the top of tilted fault blocks overlain by Miocene sediments; these palaeo-highs (buried hills) developed during a period of Neogene rifting. Smaller subeconomic discoveries have been also made in Miocene clastics and limestones (Merten 2006). The Amposta oil field was discovery by Shell España in 1970, and began producing oil in 1973.

Excellent secondary porosity was formed by deep karstification during the Palaeogene exposure; intense fracturing brecciation and dolomitization also promoted porosity enhancement (Orlopp 1988). In the Mediterranean region, the Mesozoic-Tertiary boundary developed as a posttectonic unconformity after the main phase of the Palaeogene

Alpine orogeny. It is a multiple, composite unconformity formed by superposition, or stacking, of several Palaeogene and Miocene unconformities that truncate the fractured Mesozoic carbonate sequences at various depths. Upper Jurassic and Lower Cretaceous carbonate sequences are well exposed onshore and varied degrees of karstification are common in outcrops, depending on their subaerial exposure period. These carbonate beds have caves, solution-enlarged fractures, vuggy porosity and large caverns, very similar to those documented in the nearby Amposta field (Watson 1982). Several palaeokarst horizons developed from presumed Lower Eocene (Esteban & Klappa 1983) and related to sedimentary discontinuities have been recognized onshore (Esteban 1973; Esteban & Julià 1973), only slightly modified by present-day karstic processes. Karst is as old as late Cretaceous in the offshore zone (Esteban 1991). Well-preserved examples of karstic dissolution have been described in the neighbouring Casablanca oil field (Esteban 1991; Lomando et al. 1993) and in the onshore Catalan Coastal Ranges (Esteban 1973; Calvet et al. 1983; Klimowitz et al. 2005).

In this paper, the different cements, fractures and stylolites and karstic sediments are described for the main oil reservoir rock of Amposta Marino C2 well from the Amposta field. The fluid flow history before, during and after oil migration is inferred from petrological and geochemical characterization of the different cements. The main questions being addressed are thus:

(1) How many fracturing events have affected these carbonate reservoirs and when did they occur in relation to the tectonic evolution of the basin?
(2) How many generations of fracture-filling cements can be identified and how do they relate to the fracturing events?
(3) Were the fracture-filling cements internally- or externally-derived (open or closed-system diagenesis)?
(4) What are the sources of formation water that facilitated cementation of fractures; meteoric water, deep basin water, etc.?

GEOLOGICAL FRAMEWORK

The Amposta oil field is located in the Valencia Trough (northern Gulf of Valencia, NW Mediterranean), stretching between the eastern Iberian Peninsula and the Balearic Islands, at 22 km offshore south of the Ebro delta (Fig. 1). The Catalan Coastal Ranges constitute the western boundary of the Valencia Trough. The regional structure of the western Mediterranean area is a direct consequence of the Neogene (late Oligocene-early Miocene) extensional tectonic activity. The Valencia Trough displays a well-developed horst and graben structure with a general NE-SW trend. Pre-Neogene tectonic structures are difficult to recognize in the Gulf of Valencia. The NE-SW rift units are limited by transverse NW-SE faults with a marked strike-slip component (high-relief accommodation
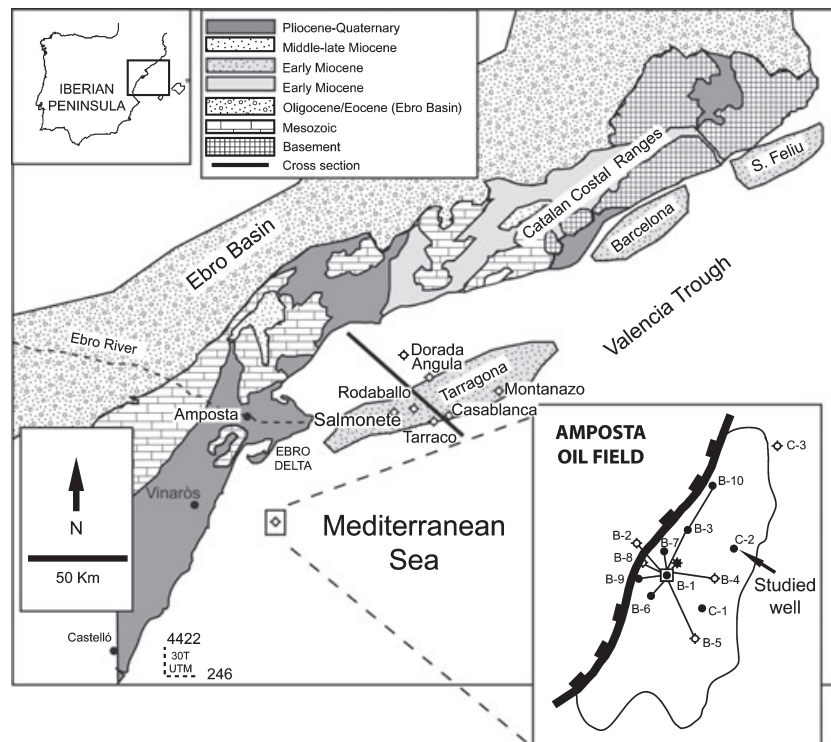

Fig. 1. Simplified geological map of the Catalan Costal Ranges and location of the main oil fields in the Valencia Trough (western Mediterranean Sea), showing the detail of the Amposta oil field and drilled wells. Location of the studied well (C-2, Amposta Marino well) (adapted from Losantos et al. 1989).

zones). The exposed up-thrown ridges in the Catalan Coastal Ranges are very similar to the Valencia Trough graben system buried beneath the Neogene sediments offshore (Roca *et al.* 1999; Vegas & de Vicente 2004). The Amposta oil field is located in an elongated tilted bloc of Mesozoic carbonates (25 km long), dipping toward the ESE at 20° (Fig. 2A). The western margin is bounded by a major extensional fault, which has a NE-SW direction parallel to the shoreline, and with a throw in excess of 1000 m (Seemann *et al.* 1990).

A thick sedimentary succession is recorded above the Hercynian basement; this constitutes a largely deformed Palaeozoic–Mesozoic sequence and Neogene-Quaternary cover, separated by an important erosive surface (Fig. 2B).

Two major rifting stages occurred during the Mesozoic (Salas & Casas 1993; Salas *et al.* 2001). The first stage affected the Upper Permian and Triassic units (red beds, siliciclastics, carbonates and evaporites), whereas the second stage affected the Jurassic to Lower Cretaceous limestones. The Upper Cretaceous units are not preserved in the study area.

Part of the Valencia Trough and the present Catalan Coastal Ranges were uplifted during the regional Palaeogene contraction (Gaspar-Escribano *et al.* 2004). During this period (late Eocene-early Oligocene), Mesozoic carbonates were uplifted and intensively eroded. Later, during the late Oligocene-early Miocene, the compressional structures were overprinted by extensional faulting related to a regional rifting stage, giving rise to the NE-SW trending structures. Although some areas (e.g. Barcelona offshore graben) contain basal Palaeogene continental facies (Martinez del Olmo & Esteban 1983), the transitional and marine Neogene sediments (synrift and postrift) were mostly deposited directly and unconformably up on the Mesozoic basement in the Valencia Trough. Compressive inversion of previous normal faults together with the Mediterranean Sea level dropping during the Messinian resulted in a new phase of extensive erosion. The Plio-Quaternary sandstones and clays from the Ebro Group were deposited unconformably over the Miocene clastics of the Castellon Group (Fig. 2).

METHODS

About 23 samples from Amposta Marino C-2 well, at true vertical depth (TVD) between 1874 and 1957 m below sea level (Table 1, Fig. 3) were collected for petrological and geochemical studies of the host-limestones and cements filling fractures and stylolites. Standard thin sections were examined using optical, cathodoluminescence (Technosyn Cold Model 8200 MkII; 16–19 kv and 350 μA) and fluorescence microscopes (Nikon equipped with a blue-violet incident light excitation filter). X-ray diffraction (Siemens D-500 with secondary graphite-mono-

chromatograph operating at 40 kv and 30 mA) was used for identification of the main mineral phases.

The samples were carefully selected following the petrological study in order to characterize the geochemical composition of the different cement phases. Carbon-coated thin sections were analysed using a CAMECA SX-50 microprobe equipped with four vertically-displayed WD X-ray spectrometers and operating at 20 kV of excitation potential, 10 μm of beam diameter and 10 nA of current intensity for the Ca and Mg analysis and 50 nA for Mn, Fe, Sr and Na. The detection limits are 440 ppm for Ca, 380 ppm for Mg, 350 ppm for Mn, 340 ppm for Fe, 209 ppm for Sr and 240 ppm for Na. Analytical precision of the major elements averaged 6% standard error at 3σ confidence level.

For carbon and oxygen stable isotope determinations, 100–500 μg of 66 host-limestones and calcite cements were obtained using a dental microdrill. Samples were reacted with 103% H_3PO_4 for 2 min in vacuum at 70°C. The CO_2 was analysed using an carbonate Kiel device connected on-line to a Finnigan MAT252 mass spectrometer. The values, expressed in per mil with respect to the Vienna Pee Dee Belemnite (VPDB) standard, had a precision of ±0.02‰ VPDB for $\delta^{13}C$ and ±0.08‰ VPDB for $\delta^{18}O$.

For $^{87}Sr/^{86}Sr$ ratio analyses, 14 samples were microdrilled and analysed in the CAI of Universidad Complutense de Madrid. The powdered samples were converted to chlorides by leaching them several times in HCl 2.5N. The final liquid samples were loaded into a cation exchange column with DOVEX 52Wx12 200/400 mesh resin and the strontium separates were analysed with a VG Sector 54 TIMS, previously loaded onto a Ta filament. The standards and reference samples used, NBS-987, averaged 0.710255 (n = 9), indicating a weighted reproducibility within the range of ±4 × 10^{-5}. The analytical accuracy was 0.01%. All the results were normalized to $^{87}Sr/^{86}Sr$ = 0.1194.

Four pyrite samples, 150–350 μg, were analysed for their $\delta^{34}S$ composition. The SO_2 gasses produced by the sulphides were analysed on a continuous-flow elemental-analyser Finnigan DELTA plus XP mass spectrometer with Finnigan Mat CHN 1108 analyser for sulphur. The values are given relative to the VCDT (Vienna Cañon Diablo Troilite) reference, offering precision of ±0.4‰.

LOWER CRETACEOUS HOST-LIMESTONES

The host-limestones (usually brecciated) are wackestones to packstones with dull-red luminescence and red blue fluorescence. They are mainly composed of marine fauna, such as benthic foraminifera, silicified sponge spicules, and echinoderm fragments. Foraminifera consist principally of *Orbitolinopsis, Nautiloculina, Pseudocyclamina* and *Choffatella*, and miliolids, as well as green algae. The uppermost part of the sampled interval (sample 1874) is a wackestone characterized by freshwater facies (girogonites of
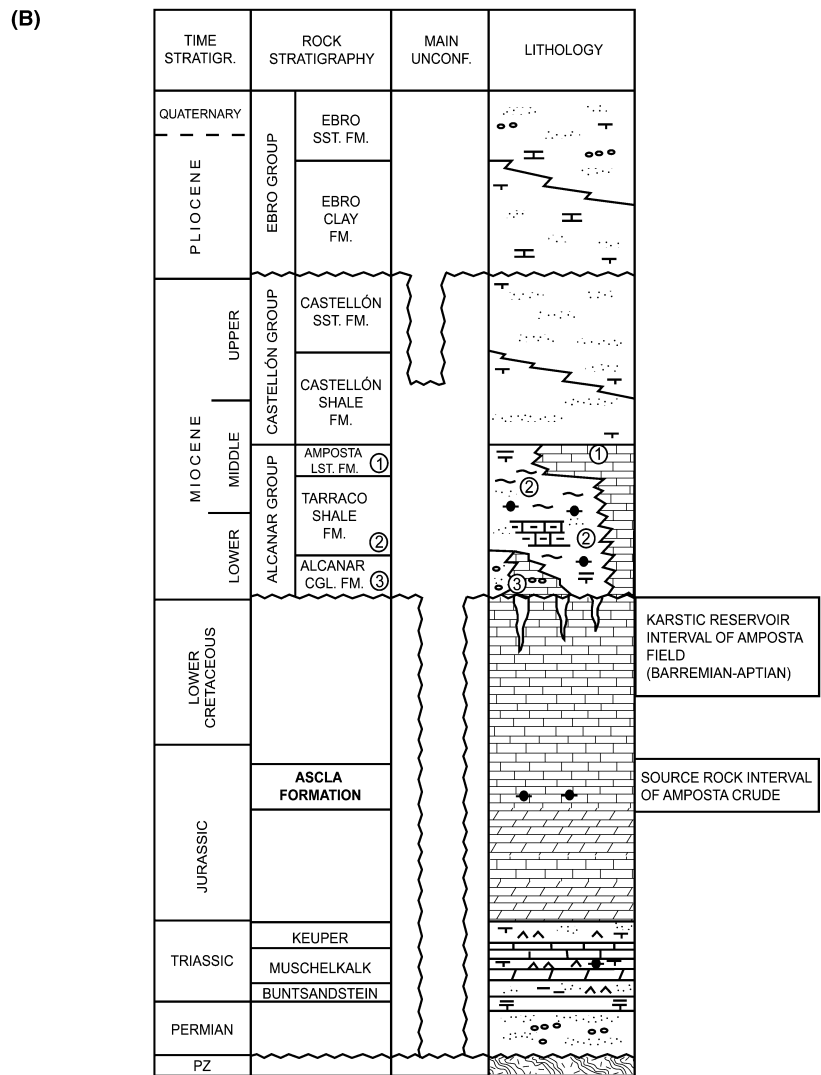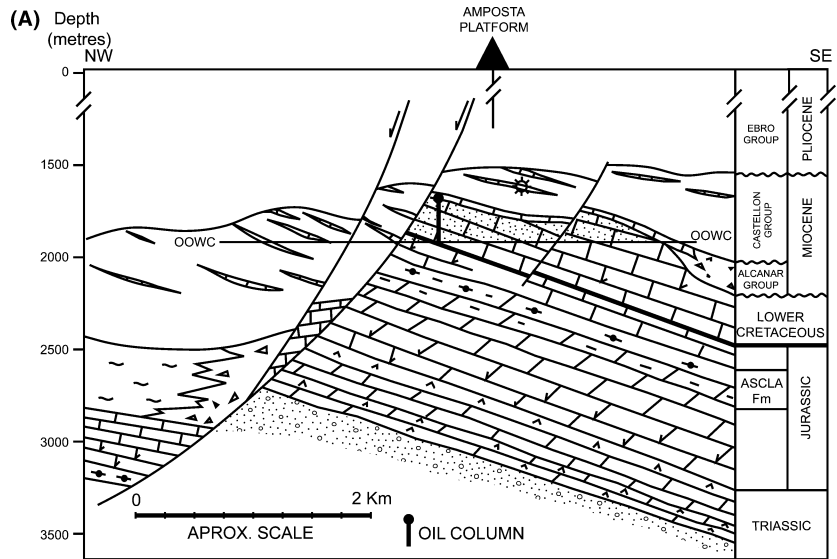
Fig. 2. (A) Geological cross-section of the Amposta field. (B) Stratigraphy of the Amposta oil field. Slightly modified from Seemann *et al.* (1990).

Table 1 Observed fracture, cement and stylolite types and presence of kaolinite, pyrite (in fractures type C), barite and oil in the studied samples of the Amposta Marino C-2 well.

| Sample (Depth, m.) | Fracture type | | | Randomly oriented stylolites | Cement/sediment type | | | | | Barite | Kaolinite | Pyrite (in fractures) | Oil |
	A	B	C		CC1	CC2	CS3r	CS3g	CC4				
1874	x	x	x	x	x	x		x	x				x
1893.3			x	x					x		x (CC4)		x
1895.5			x	x					x			x	x
1896			x	x					x				x
1906			x	x					x		x (CC4)		x
1908.8			x						x			x	
1909.5			x				x		x				
1910.3	x		x	x	x			x	x			x	
1910.8	x		x	x	x				x		x (CC4)		x
1942	x		x	x	x				x				x
1943.5			x						x		x (CC4)		
1944.6	x		x		x			x	x			x	
1945.8			x					x	x			x	
1951.4	x		x	x	x				x		x (CC4)		
1952.6	x	x	x	x	x	x		x	x		x (CS3)	x	
1952.7	x		x		x			x	x		x (CS3, CC4)	x	
1954.3	x		x	x	x		x		x			x	
1957			x	x			x		x	x		x	

CC1, non-luminescent calcite cement 1; CC2, blocky non to dull-red luminescent calcite cement 2; CS3r, reddish microsparite calcite sediment 3; CS3g, greenish microsparite calcite sediment 3; CC4, blocky calcite cement 4.

charophytes –*Atoporochara*- and ostracods), and shallow marine dasycladacean algae. Small framboidal pyrites are disseminated in the host-limestones or concentrated in the stylolitic planes, as insoluble residue.

The reservoir interval is dated as Valanginian to Aptian (Seemann *et al.* 1990); the presence of *Atoporochara* and *Orbitolinopsis* indicates a Barremian–Aptian age (Hardenbol *et al.* 1998).

The marine limestones and the uppermost brackish carbonate facies do not reveal significant differences in their minor and trace element contents, except for the Fe contents (Table 2, Fig. 4). The host-limestones are characterized by Mg, Sr and Na contents from 1015 to 4910 ppm, between 355 and 1410 and up to 435 ppm, respectively; Mn contents are below detection limit in all cases. Fe content display higher values in the uppermost brackish facies than in the marine limestones (from 875 to 1815 ppm, and up to 560, respectively; Table 2). Oxygen isotopic compositions range from −4.2 to −2.2 ‰ VPDB, and $\delta^{13}C$ between +0.9 and +1.5 ‰ VPDB (Table 3, Fig. 5).

The $^{87}Sr/^{86}Sr$ ratios of the limestones range from 0.70748 to 0.70763 (mean value of 0.70755; Table 4; Fig. 6).

FRACTURE TYPES, CEMENTS AND STYLOLITES

Three main types of fractures, related to specific calcite cement or sediment infillings (Table 1, Fig. 7) have been identified.

Fracture type A and calcite cement 1 (CC1)

Fractures of type A are part of the oldest fracture system. These fractures are vertical to subvertical, thin fractures (1–3 mm thick) with straight walls, totally occluded by calcite cement 1 (CC1) (Fig. 8A,B).

The CC1 constitute anhedral non-luminescent calcite crystals, from 15 to 120 μm in size (Fig. 8G,H). These calcite cements are characterized by Mg from 3625 to 6320 ppm, Sr from 345 to 1400 ppm, Fe up to
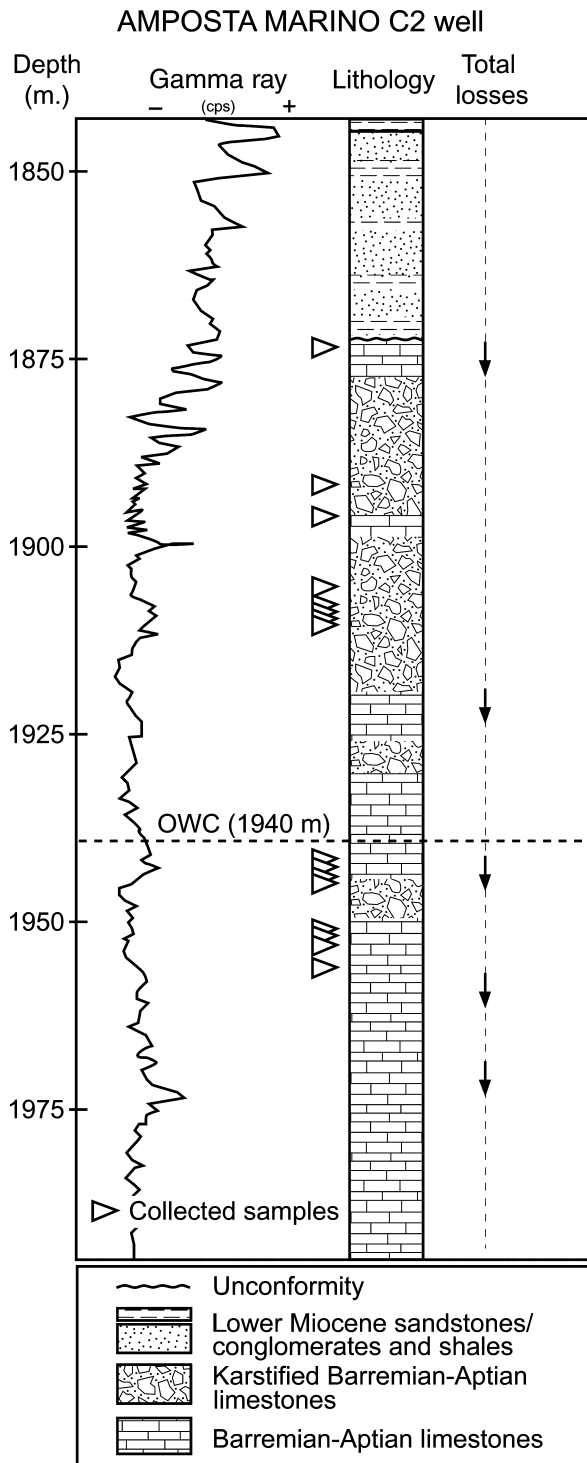
AMPOSTA MARINO C2 well

Fig. 3. Schematic section of the Amposta Marino C2 well showing the position of the studied samples, the oil water contact (OWC; after Seemann *et al.* 1990), the Gamma Ray log and the location of the total losses (Courtesy of Escal UGS s.l.).

3995 ppm and Na up to 255 ppm (Mn content is below detection limit) (Table 2). Oxygen and carbon isotopic compositions offer a wide range of values (between −9.4

and −5.9‰ VPDB for oxygen and from −4.4 to +1.3‰ VPDB for carbon), depending on the samples and evidence that several generations of cements (and possible deformation events) are recorded in these fractures (Table 3, Fig. 5).

Fracture type B and calcite cement 2 (CC2)

Fractures of type B are horizontal to subhorizontal fractures from less than 1 mm to 3 cm width. Subhorizontal stylolite planes affect the walls of these fractures (the walls of the fractures are the later location of the stylolites; Fig. 8E). They are totally occluded by the calcite cement 2 (CC2) (Fig. 8A,E).

The CC2 is made of white to brownish, anhedral to subhedral, blocky calcite crystals, non to dull-red luminescent and red blue fluorescent (as is the host-rock). Calcite crystals show cloudy appearance due to solid inclusions with marked cleavage planes and sizes ranging between 300 μm and 2 mm. CC2 is characterized by Mg from 710 to 2730 ppm, Sr from 555 to 1480 ppm, Fe between 340 and 1660 ppm, and Na and Mn up to 455 and 385 ppm, respectively (Table 2, Fig. 4). The oxygen and carbon isotope compositions of these calcite cements range from −8.9 to −5.1 ‰ and from +0.1 to +1.1 ‰ VPDB, respectively (Table 3, Fig. 5). The $^{87}Sr/^{86}Sr$ ratios range from 0.70744 to 0.70762 (average value of 0.70751; Table 4; Fig. 6).

Fracture type C, calcite sediment 3 (CS3) and calcite cement 4 (CC4)

Fractures of type C are vertical to subvertical and crosscut both fractures A and B. The fracture type C displays sharp and undulating walls, locally enlarged by dissolution, and are totally or partially filled by calcite sediment 3 (CS3) and calcite cement 4 (CC4) (Fig. 8A,B). Locally these fractures are wedge-shaped (with a maximum width of 2 cm; Fig. 8B). Minor porosity remains even after CC4 precipitation.

The CS3 is constituted of reddish (CS3r) and greenish (CS3g) microsparite calcite sediment and clay minerals. Individual calcite crystal sizes ranges between 8 and 40 μm. This generation shows dull orange to bright orange luminescence and red blue fluorescence. The CS3r partially filled the original fracture porosity; it displays a geopetal distribution locally, where the upper part of the fracture is occluded by CC4 (Fig. 8B,F). The reddish CS3r records Mg and Sr from 2620 to 4040 ppm and 640 to 1055 ppm, respectively. Recorded Fe and Na are up to 720 and 385 ppm, respectivlely, while Mn is below detection limit (Table 2, Fig. 4). The oxygen and carbon isotope compositions range from −9.9 to −5.6 ‰ VPDB and from −1.4 to +0.3 ‰ VPDB, respectively (Table 3, Fig. 5). The strontium isotope compositions range from 0.70857 to 0.70888 (average value of 0.70871), which are

Table 2 Summary of trace element composition of host-limestones, calcite cements and calcite infillings in the Amposta Marino C2 well.

Generation	Ca (ppm)	Mg (ppm)	Sr (ppm)	Fe (ppm)	Na (ppm)	Mn (ppm)	Mg/Ca molar ratio (fluid)*,†		Sr/Ca molar Ratio (fluid)‡	Ca/Fe molar ratio (fluid)§
Brackish host-limestones										
m	377858	1013	658	875	<b.d.l.	<b.d.l.	0.35	0.04	0.0128	1536
M	399645	4766	1261	1813	391	<b.d.l.	1.68	0.17	0.0247	3097
mv (n = 5)	391250	2755	928	1192	–	–	0.97	0.10	0.0181	2453
SD	8555	1369	253	423	–	–	0.49	0.05	0.0052	669
Marine host-limestones										
m	390383	1784	355	<b.d.l.	<b.d.l.	<b.d.l.	0.61	0.06	0.0069	-
M	399870	4909	1407	561	436	<b.d.l.	1.72	0.18	0.0275	6150
mv (n = 15)	394159	3407	887	–	–	–	1.19	0.12	0.0172	-
SD	3096	880	273	–	–	–	0.31	0.03	0.0053	-
CC1										
m	387374	3625	343	<b.d.l.	<b.d.l.	<b.d.l.	1.25	0.13	0.0068	–
M	397524	6317	1397	3995	255	<b.d.l.	2.23	0.23	0.0272	7726
mv (n = 16)	393107	4431	920	–	–	–	1.55	0.16	0.0178	–
SD	2876	760	250	–	–	–	0.27	0.03	0.0048	–
CC2										
m	395417	712	553	340	<b.d.l.	<b.d.l.	0.25	0.03	0.0105	1669
M	400086	2731	1479	1660	453	383	0.94	0.10	0.0284	8189
mv (n = 10)	398545	1924	983	658	–	–	0.66	0.07	0.0188	5625
SD	1540	628	363	505	66	–	0.22	0.02	0.0070	2354
CS3r										
m	392466	2619	640	<b.d.l.	<b.d.l.	<b.d.l.	0.91	0.09	0.0124	–
M	398229	4038	1053	721	383	<b.d.l.	1.41	0.15	0.0203	6115
mv (n = 9)	394982	3426	863	–	–	–	1.19	0.12	0.0167	–
SD	1861	558	154	–	–	–	0.20	0.02	0.0030	–
CS3g										
m	386649	1052	491	<b.d.l.	<b.d.l.	<b.d.l.	0.37	0.04	0.0095	–
M	395067	5461	1259	2701	256	<b.d.l.	1.94	0.20	0.0243	3941
mv (n = 9)	391864	3692	866	–	–	–	1.30	0.13	0.0168	-
SD	2627	1446	252	–	–	–	0.51	0.05	0.0048	–
CC4										
m	380264	390	477	<b.d.l.	<b.d.l.	<b.d.l.	0.14	0.01	0.0092	–
M	404536	10453	1579	3032	435	469	3.78	0.39	0.0302	11782
mv (n = 87)	394847	3224	906	–	–	–	1.13	0.12	0.0175	–
SD	4262	1806	251	–	–	–	0.64	0.07	0.0048	–

m, minimum value; M, maximum value; mv, mean value; n, number of analysed spots in the same sample; sd, standard deviation; b.d.l., below detection limit. See legend in Table 1 for CC1, CC2, CS3 and CC4.
*Using KMg = 0.012 (at 25°C) (Burton & Walter 1991; Mucci 1987; Mucci & Morse 1983).
†Using KMg = 0.1163 (at 90°C) (Katz 1973).
‡Using KSr = 0.06 (at 25, 40, 98, 200°C) (Katz *et al.* 1972; Stoessell *et al.* 1987).
§Using KFe = 5 (Dromgoole & Walter 1990).

more radiogenic than those of the host-rock and CC2 (Table 4, Fig. 6).

Clasts of host-limestones can be found within CS3g (Fig. 9A). Mg and Sr of CS3g vary from 1050 to 5460 ppm and from 490 to 1260 ppm; Fe and Na are up to 2700 and 255 ppm, respectively, while Mn is below detection limit (Table 2, Fig. 4). CS3g shows $\delta^{18}O$ values ranging from −8.7 to −4.1 ‰ VPDB, and $\delta^{13}C$ between −1.2 and +0.5 ‰ VPDB (Table 3, Fig. 5). Only one $^{87}Sr/^{86}Sr$ value was measured in CS3g, giving a 0.70861 ratio (Table 4, Fig. 6). Carbon and strontium isotope compositions of CS3g are very close to those of the CS3r, while their $\delta^{18}O$ values are slightly lower.
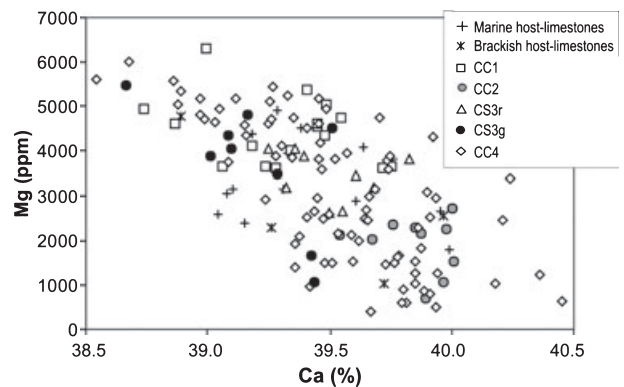

Fig. 4. Plots of Mg versus Ca contents in the host-limestones and calcite cements-sediments. See legend in Table 1 for CC1, CC2, CS3 and CC4.

The CC4 generation is the most volumetrically-significant of all fracturing-filling cements. In general, it occurs as limpid white calcite crystals, filling the fractures (Figs 8B, 9D). CC4 is composed of two cement generations (Fig. 8J):

(1) Isopachous-rim cement generation made of subhedral to euhedral calcite crystals, 15 to 80 µm in size and with orange-bright luminescence. The larger crystals display a non-luminescent nucleus, dark in plane light, with an orange to yellow-bright luminescent outer zone.

Table 3 Oxygen and carbon isotopic compositions of the host-limestones and the calcite cements.

Generation	Depth (m)	Label	$\delta^{18}O$ ‰ VPDB	$\delta^{13}C$ ‰ VPDB
Marine host-limestones	1942	6d	-2.22	+1.14
	1942	6e	-2.32	+1.05
	1910.3	8h	-2.92	+1.37
	1942	10b	-3.57	+1.36
	1944.6	12f	-3.27	+0.88
	1944.6	12g	-3.59	+0.88
	1951.4	14c	-3.93	+1.50
	1952.6	15g	-2.72	+1.42
	1957	18d	-4.21	+0.96
	1957	18e	-3.46	+1.23
CC1	1952.7	16c	-5.87	-3.49
	1952.7	16d	-6.36	-4.38
	1952.7	16e	-9.37	+1.26
CC2	1874	1a	-7.69	+0.47
	1874	1b	-5.15	+0.53
	1874	1c	-7.26	+0.55
	1874	1d	-7.77	+0.13
	1874	1f	-8.94	+0.31
	1952.6	15b	-8.31	+0.72
	1952.6	15c	-8.90	+1.14
CS3r	1954.3	17a	-9.85	+0.32
	1957	18b	-8.38	-1.40
	1957	18c	-9.91	-0.77
	1957	19a	-5.64	-0.72
	1957	19b	-5.77	-0.35
	1957	19c	-8.87	+0.34
CS3g	1910.3	8i	-5.83	-0.08
	1910.3	8j	-8.66	-0.59
	1944.6	12a	-8.59	+0.01
	1952.6	15a	-5.87	-1.20
	1952.6	15f	-4.07	-0.58
	1952.6	15h	-4.09	-0.27
	1952.7	16b	-4.41	+0.45

Table 3 (Continued).

Generation	Depth (m)	Label	$\delta^{18}O$ ‰ VPDB	$\delta^{13}C$ ‰ VPDB
CC4	1895.5	4a	-11.23	+0.61
	1942	6a	-13.25	+0.50
	1942	6b	-12.99	+0.73
	1942	6c	-13.01	+0.45
	1909.5	7a	-13.33	+0.31
	1910.3	8c	-11.73	+0.31
	1910.3	8d	-13.17	+0.47
	1910.3	8f	-12.86	+0.49
	1910.3	8g	-13.55	+0.22
	1910.8	9a	-13.04	+0.46
	1910.8	10a	-12.77	+0.43
	1910.8	10c	-13.15	+0.41
	1943.5	11a	-11.21	+1.22
	1943.5	11b	-12.45	+0.80
	1944.6	12c	-12.29	+0.28
	1944.6	12d	-11.87	+0.83
	1944.6	12e	-12.77	+0.68
	1952.6	15d	-12.68	+0.67
	1952.6	15e	-12.68	+0.54
	1952.7	16a	-12.69	-0.20
	1952.7	16f	-12.04	+0.38
	1952.7	16g	-13.13	+0.38
	1954.3	17f	-12.04	+0.27
	1954.3	17b	-12.71	+0.62
	1954.3	17c	-13.01	+0.47
	1954.3	17d	-12.44	+0.36
	1954.3	17e	-11.99	+0.91
	1957	19d	-11.95	+0.69
	1957	19e	-12.34	+0.46
	1910.3	21a	-12.75	+0.65
	1910.3	21b	-12.68	+0.71
	1910.3	21c	-12.09	+0.56
	1910.3	21d	-10.24	+1.11

See legend in Table 1 for CC1, CC2, CS3 and CC4.

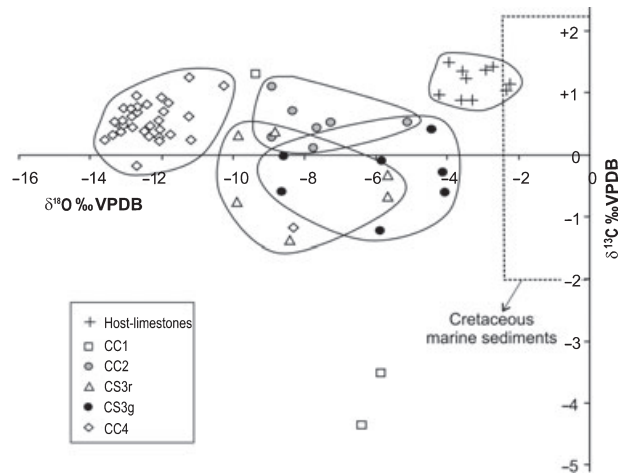**Fig. 5.** $\delta^{18}O$ and $\delta^{13}C$ values of the host-limestones and calcite cements-sediments. Range of values for Cretaceous seawater after Veizer & Hoefs (1976) and Jenkyns *et al.* (2002). See legend in Table 1 for CC1, CC2, CS3 and CC4.

Table 4 Strontium isotopic compositions of the host-limestones and the calcite cements. See legend in Table 1 for CC1, CC2, CS3 and CC4.

Generation	Depth (m)	Label	$^{87}Sr/^{86}Sr$
Marine host-limestones	1908.8	6A	0.707633±5
	1910.3	8B	0.707524±5
	1957	18A	0.707483±5
CC2	1874	1A	0.707483±5
	1874	1B	0.707436±5
	1952.6	15C	0.707616±6
CS3r	1954.3	17B	0.708699±5
	1957	19A	0.708576±5
CS3g	1952.6	15A	0.708615±5
CC4	1910.3	8A	0.708995±6
	1943.5	11C	0.709273±5
	1944.6	12B	0.709129±5
	1952.7	16A	0.709166±5
	1954.3	17A	0.709100±5

(2) Blocky anhedral to subhedral calcite crystals with dull-red luminescence and red blue fluorescence, up to 1 mm in size, locally zoned with a dark nucleus (dull-red luminescent) and a dull orange to yellow luminescent outer zone. Outer borders of calcite crystals are rounded and appear to be corroded, indicating a dissolution event postdating CC4 precipitation (Figs 8I, 9C,E).

CC4 is characterized by Mg from 390 to 10450 ppm and Sr between 475 and 1580 ppm; recorded Fe, Na and Mn lower than 3030 ppm, 435 ppm and 470 ppm, respectively (Table 2, Fig. 4). The $\delta^{18}O$ and $\delta^{13}C$ values of the blocky calcite cement vary between −13.5 and −10.2 ‰

VPDB, and from −0.2 to +1.2 ‰ VPDB, respectively. This cement generation records the lowest oxygen isotope ratios, being about 5‰ lower than the $\delta^{18}O$ values of the rest of the calcite cements and about 8‰ lower than the host-rock (Table 3, Fig. 5). The $^{87}Sr/^{86}Sr$ ratios vary between 0.70899 and 0.70927, with an average value of 0.70913; these cements are somewhat more radiogenic than the CS3, and significantly more radiogenic than the host-rock and the CC2 (Table 4, Fig. 6).

Kaolinite, barite and pyrite are frequently associated with CC4. Kaolinite occurs with a booklet texture and has bright blue luminescence patterns and bright white fluorescence (Fig. 8G,H). Kaolinite patches are pore-filling after CC4 precipitation, thus postdating CC4 (Fig. 9C), but it is locally engulfed by overgowths of CC4 (Fig. 9D). Kaolinite is commonly impregnated by oil (Fig. 9C). Barite occurs very locally as prismatic crystals forming aggregates (Fig. 9F). Pyrite occurs as millimetric crystal aggregates, 1–2 mm in size (Fig. 8A); in some cases, the pyrite crystals show pseudo-skeletal habit. Sulphur isotope compositions of aggregates of euhedral crystals (fracture-related) oscillate from −16.7‰ to −12.9‰ VCDT (Table 5). Both pyrite and barite postdate CC4.

Stylolites

At least two generations of stylolites occur in the studied samples. The oldest stylolite system cross-cuts fracture type A. The second, and most abundant, stylolite system are constituted by mostly-open and randomly-oriented stylolites (from subhorizontal to subvertical), giving the rock a pseudo-nodular texture. This second generation of stylolites postdates CC1 and CC2 cements, but display ambiguous relationships with fractures type C, thus tentatively indicating a coeval origin. Subhorizontally oriented stylolites, which can occur as the walls of the fracture type B (Fig. 8E), have also been attributed to this pseudo-nodular texture between the randomly oriented stylolites. Subhorizontal and randomly oriented stylolites were open but CC4 cement, together with oil, has partially filled this open stylolitic porosity (Fig. 8C).

OIL, CEMENT AND POROSITY RELATIONSHIPS

Non-luminescent and brown-fluorescent oil occurs in partially-occluded type C fractures and stylolites and in the host-limestones. Thus, oil emplacement was post-CC4 precipitation. Where the fractures of type C are more-or-less totally occluded by CC4, oil is only found in the middle of the fracture, following the intercrystalline contacts and/or along cleavage planes (Fig. 9B). Locally, oil impregnates the host-limestones; in such cases, oil is present only close to fractures or stylolites (which also contain oil;
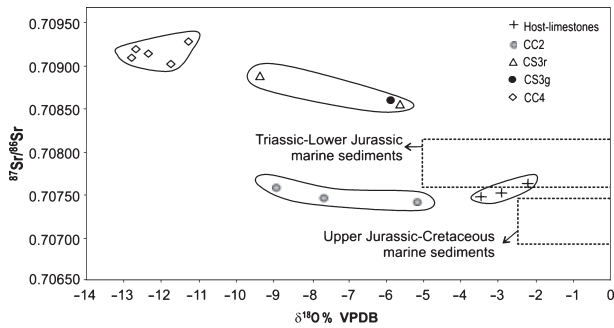
Fig. 6. $^{87}Sr/^{86}Sr$ ratio of the host-limestones and calcite cements-sediments. Range of values for Upper Jurassic-Cretaceous seawater after Veizer & Compston (1974), Burke *et al.* (1982), Koepnick *et al.* (1985), Jones *et al.* (1994), Veizer *et al.* (1997) and Jenkyns *et al.* (2002). See legend in Table 1 for CC1, CC2, CS3 and CC4.

Fig. 8C,D,E), suggesting that oil circulated preferentially along these planes and that fracture porosity and stylolite porosity were interconnected.

DISCUSSION

Diagenesis of the host-limestones

When precipitation occurs in equilibrium, the chemical composition of the fluid from which calcite precipitates is related to the chemical composition of the precipitate, and can be determined by using the distribution coefficient equation of McIntire (1963) (i.e., Meyers & Lohmann 1985; Banner & Hanson 1990). Although some studies (Reeder & Grams 1987; Paquette & Reeder 1995) have shown that minor element distribution in natural carbonates does not always reflect equilibrium partitioning; in this study, we assume that precipitation occurred in equilibrium.

The molar ratios of Sr/Ca and Ca/Fe of the host marine limestone are consistent with precipitation from formation waters whereas the molar ratios of Mg/Ca are consistent with precipitation from either meteoric or formation waters (Table 2; Skougstad & Horr 1963; Kinsman 1969; McIntire 1963; Tucker & Howson *et al.* 1987; Tucker & Wright 1990). Formation waters are here defined as waters initially trapped during sedimentation that changed their composition during basin evolution due to diagenetic reactions (after Lawrence & Cornford 1995). The molar ratios of Sr/Ca of the uppermost brackish host-rock are characteristic of being precipitated from formation waters, whereas the molar ratios of Ca/Fe indicate the influence of meteoric waters; the molar ratios of Mg/Ca indicate either precipitation from meteoric or formation waters.

The analysis of minor and trace elements in the marine and in the uppermost brackish host-limestones does not seem to record unequivocal evidence of their marine and brackish origins (Table 2). The $\delta^{18}O$ of the limestones are
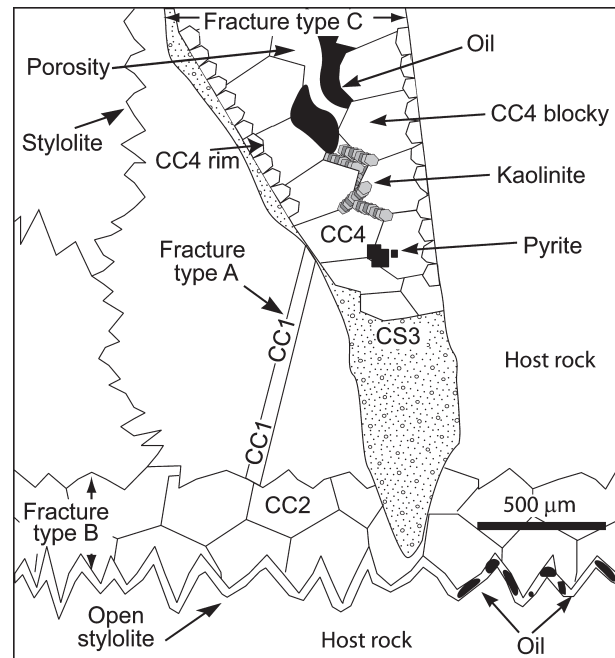
Fig. 7. Relationships of fractures, cements–sediments, stylolites and oil. See legend in Table 1 for CC1, CC2, CS3 and CC4.

slightly lower than the expected values for limestones precipitated from Cretaceous seawater (from −2.5 to +1 ‰ VPDB), and the carbon isotope compositions match well with those of the Cretaceous seawater (ranging from −2 and +3‰ VPDB; Veizer & Hoefs 1976; Jenkyns *et al.* 2002) (no data are available for the brackish limestones; Fig. 5). Strontium ratios are slightly more radiogenic than those of the Upper Jurassic-Lower Cretaceous seawater (0.7068–0.7074; after Veizer & Compston 1974; Burke *et al.* 1982; Koepnick *et al.* 1985; Jones *et al.* 1994; Veizer *et al.* 1997; Jenkyns *et al.* 2002; Fig. 6). These data show that the original marine and brackish signals have been overprinted during diagenesis.

Relationships between fracturing events and palaeofluids

Pre-Alpine fractures and calcite cement 1 (CC1).
Pre-Alpine fractures (fracture type A) occur as vertical to subvertical thin fractures, which represent several, undifferentiated, fracturing events. A large range of variation in the oxygen isotope compositions of the CC1 supports this multistage interpretation (Fig. 5).

Palaeogene compressional fractures and calcite cement 2 (CC2).
During the Palaeogene Alpine compression, the horizontal fractures (type B) were developed (Figs 10 and 11). Fractures are totally occluded by blocky calcite cement (CC2).

The molar ratios of Mg/Ca, Sr/Ca and Ca/Fe of CC2 in fractures type B are consistent either with precipitation from meteoric or formation waters.

The similarity between the $\delta^{13}C$ values of CC2 and those of the host-rock (Fig. 5) is probably due to the buffering of the pore-water carbon isotopic composition by extensive dissolution of the host-limestones (Marshall 1992). The presence of abundant stylolite surfaces within the host-limestones provides evidence of this dissolution process.

The similarity between the $^{87}Sr/^{86}Sr$ ratios of the CC2 and those of the host-rock (Cretaceous host marine limestones; Fig. 6), together with the $\delta^{13}C$ values, indicate a high degree of fluid-rock interaction in a closed palaeohydrogeological system. Oxygen isotopic compositions are the most similar to host-limestones with respect to the other cements, thus also supporting this interpretation. Thermal modelling from the Amposta Marino C3 well (location in Fig. 1) indicates that the maximum subsidence attained by the Lower Cretaceous limestones during the Palaeogene was <1300 m; considering a geothermal gradient of 30°C km^{-1} (Salas & Permanyer 2003; Permanyer & Salas 2005), an assumed temperature of 25°C at the surface, and ruling out the inflow of externally sourced hotter fluids, the maximum precipitation temperature was, therefore, probably less than 60°C. Thus, assuming this relatively low temperature of precipitation for CC2 and applying the temperature equation of Craig (1965), calculated $\delta^{18}O$ of fluid is between −5.7 and 0‰ VSMOW (Table 6); this measurements are also consistent with meteoric or formation waters.

In summary, precipitation of CC2 in type B fractures occurred from a fluid that interacted strongly with the rock, approaching a closed-system, equilibrium composition. Similar fractures and infilling calcite cements have been observed in the Palaeogene compressive structures from the Catalan Coastal Ranges (type 2 fractures, see Travé et al. 1998).

*Neogene extensional fractures, calcite sediment 3 (CS3) and calcite cement 4 (CC4).*
The vertical fractures (type C) formed during the late Oligocene-Miocene extension after the opening of the randomly- and subhorizontally-oriented stylolites (Figs 10 and 11). Circulation of corrosive (or at least undersaturated with respect to calcite) fluids along type C fractures in the Amposta area enlarged the fracture walls and the open stylolites (formed by compaction during the pre-Neogene burial stage and opened during the uplift and unloading during mesodiagenesis). At this stage, corrosion produced irregular walls by enlarging fracture porosity. Extensive karstification of the host Lower Cretaceous limestones, including large caverns, responsible for the reservoir, probably occurred at this time, after development of type C fractures and prior to CS3 infilling.

The CS3 infilling, comprised of microsparite and clay minerals, partially fills these vertical enlarged fractures, usually in a geopetal disposition. This CS3 generation displays petrological characteristics similar to the detrital karstic carbonates described in Travé et al. (1998). According to these observations, CS3 is interpreted as originally being a residual-detrital sediment with a degree of recrystallization which increases the crystal size from mud to fine-sand. The isotopic (O, C, Sr) compositions of CS3 do not match with the underlying Triassic–Jurassic limestones and the Lower Cretaceous host-limestones (Veizer & Compston 1974; Burke et al. 1982; Koepnick et al. 1985; Pirrie & Marshall 1990; Jones et al. 1994; Grötsch & Vahrenkamp 1995; Veizer et al. 1997; Jenkyns et al. 2002; Figs 5 and 6); thus, recrystallization would have modifed the original isotopic signal. Evolution to lower oxygen isotopic compositions and more radiogenic $^{87}Sr/^{86}Sr$ ratios are expected for recrystallization processes in carbonates (Kupecz & Land 1994; Malone et al. 1994; Reinhold 1998), in accordance with the observed trends in the studied CS3 infillings. Assuming recrystallization from 25 to 50°C and applying the temperature equation of Craig (1965), it would have precipitated from waters with $\delta^{18}O$ values from −6.4 to +1.4 ‰ SMOW (Table 6). These oxygen compositions for parental fluids, the $\delta^{13}C$ compositions for CS3, which are close to 0‰, the molar ratios of Mg/Ca, Sr/Ca and Ca/Fe which are consistent with recrystallization from formation waters, and the $^{87}Sr/^{86}Sr$ ratios of the CS3 which are higher than those of the host-limestones, indicates a certain degree of interaction between the fluid and more radiogenic sediments. Input of similar fluids during the Neogene extension was interpreted in the Catalan Coastal Ranges by Travé & Calvet (2001), where the meteoric fluid was a more evolved fluid due to significant interaction with sediments coupled with an increase of the residence time in the aquifer and the reservoir effect.

Precipitation of CC4 would have reduced, but not totally occluded, the remaining porosity after CS3 stage.

Fig. 8. (A), (B), (C), (D) and (E) photographs from the most representative samples of the studied C2-Amposta Marino core. These photographs illustrate the relationships among fracture types, cements and stylolites. The white label indicates the sample depth (in metres). (F), Photomicrograph (plane polarized light) of fracture type C occluded by CS3r (in geopetal disposition) and CC4; note the irregular and sharp contact, enlarged by dissolution, between host-limestones and fracture type C. (G) and (H), Photomicrograph (plane polarized light) and cathodoluminescence image, respectively, showing fracture type A filled with non-luminescent CC1 cut by fracture type C filled with the dull-red to non-luminescent blocky CC4; note the occurrence of kaolinite postdating CC4. (I), Photomicrograph (plane polarized light) showing CC2, CC4 and porosity; note that the CC4 crystals are not idiomorphic and slightly corroded; (J), Photomicrograph (cross polarized light) showing the two stages of CC4 cementation (1, rim; 2, blocky). P, pyrite. See legend in Table 1 for CC1, CC2, CS3r, CS3g and CC4.
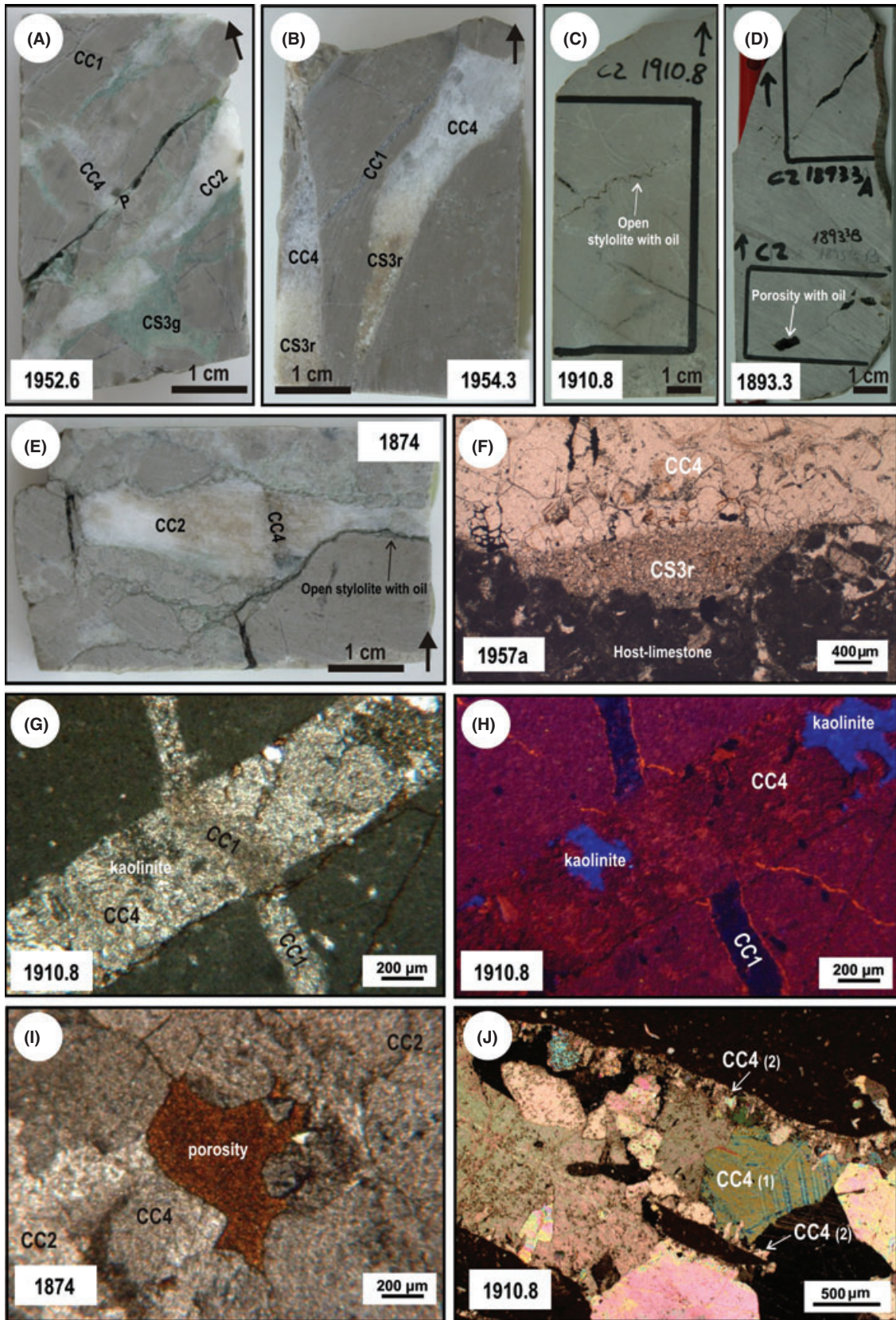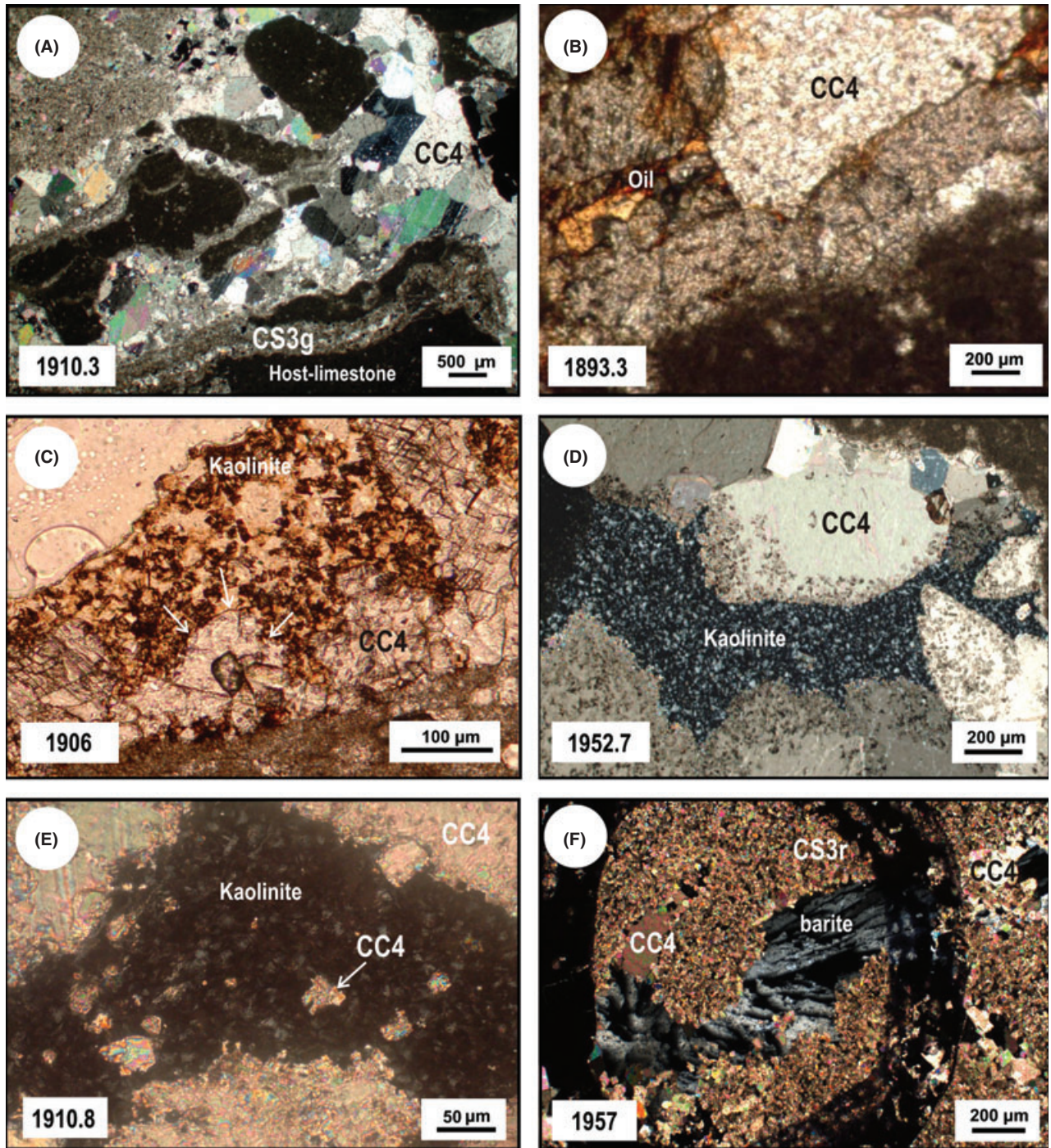
Fig. 9. Photomicrograph (cross polarized light; A, D, E, F, and plane polarized light B and C) showing: (A) fracture type C occluded by clasts of host-limestones, CS3g and CC4; (B) fracture type C cemented by blocky CC4. Oil (brownish colour) is emplaced in the intercrystalline porosity and cleavage planes of CC4; (C) and (D) patches of kaolinite postdating CC4 infilling; note the irregular and corroded borders of the calcite crystals (white arrows in C); and the engulfed kaolinite within the CC4; (E) floating calcite crystals (CC4) in the kaolinite groundmass; (F), Barite postdating CC4 in fracture type C. See legend in Table 1 for CC1, CC2, CS3r, CS3g and CC4.

Fluid inclusion within CC4 indicates that this cement precipitated at temperature between 96 and 115°C (C. Rossi, *pers. com.*). The great dispersion of the Ca, Mg, Sr, Na, Fe and Mn contents in the CC4 (Table 2, Fig. 4) indicates

that the parental fluids had variable composition. Considering temperatures higher than 90°C, the molar ratios of Mg/Ca, Sr/Ca and Ca/Fe are consistent with formation water rather than meteoric water (Table 2). Applying the

Table 5 Sulfur isotopic compositions of the pyrite in fracture-fills.

Depth (m)	Label	$\delta^{34}S$ ‰ VCDT
1910.3	8a	−14.1
1910.3	8b	−15.4
1910.3	8b(rep)	−16.7
1957	18a	−13.0

isotope equilibrium temperature equation of Craig (1965), precipitation of CC4 took place from waters with $\delta^{18}O$ values between +6.4 and +11.2‰ VSMOW (Table 6), which is in accordance with the formation water origin for the parental fluid. These heavier values are consistent with residual evaporitic brines or deep saline basinal fluids (or oil-field brines) (Montañez 1994). The occurrence of evaporites has not been described in the Jurassic to Cretaceous sequence (Seemann *et al.* 1990; Clavell & Berastegui 1991; Fig. 2). Additionally, taking into account that Jurassic to Cretaceous limestones from the Valencia Trough were mainly deposited under marine conditions, it is necessary to consider that marine-derived brines are carbonate-poor (carbonates precipitated before the sulphate stage). Therefore, it is unlikely that significant quantity of (marine) residual evaporitic brines could be responsible for CC4 precipitation, leaving deep basinal brines (i.e. high salinity formation water) as the remaining option.

Sr isotope ratios are more radiogenic values than the host-limestones and even higher than the underlying Triassic evaporites (Fig. 6), thus also excluding the influence of residual evaporitic brines but suggesting a significant source of radiogenic siliciclastic-derived allochthonous flu-

ids (i.e. external fluids) into fracture type C (Marfil *et al.* 2005). CC4 precipitation pre-dates the main oil emplacement in a buried karstic terrain, dominated by an increasingly open palaeohydrogeological system; fluids were hot, high $\delta^{18}O$ basinal and brines indicating negligible interaction with the Lower Cretaceous host-limestones (and pre-existing cements). Thus, progressive opening of the hydrogeological system within the Cretaceous limestones of the Amposta reservoir up until the main petroleum charge has been proven (Fig. 11).

Precipitation of *exotic* minerals

Kaolinite, barite and pyrite aggregates are found after CC4 precipitation. The term *exotic* (Neilson & Oxtoby 2008) has been applied to this mineral paragenesis, which is commonly interpreted as being precipitated prior, or during, arrival of petroleum (Rossi *et al.* 2001; Esteban & Taberner 2003; Salas *et al.* 2007). Exotic cementation in the Amposta samples was not massive and kaolinite, which is the most significant volumetrically, is usually oil-impregnated.

Pore-filling kaolinite patches most likely crystallized after CC4 corrosion. Engulfed kaolinite within the calcite crystals (Fig. 9D) points to a co-precipitation, but contrasting pH conditions are probably required to precipitate kaolinite and calcite, thus supporting the post-CC4 kaolinite formation. Irregular calcite borders that are in contact with kaolinite cement patches suggest that the fluids from which kaolinite precipitated were acidic (as well as bearing Si and Al) and thus caused partial dissolution of CC4 calcite. When kaolinite is present as pore-filling mineral in lime-
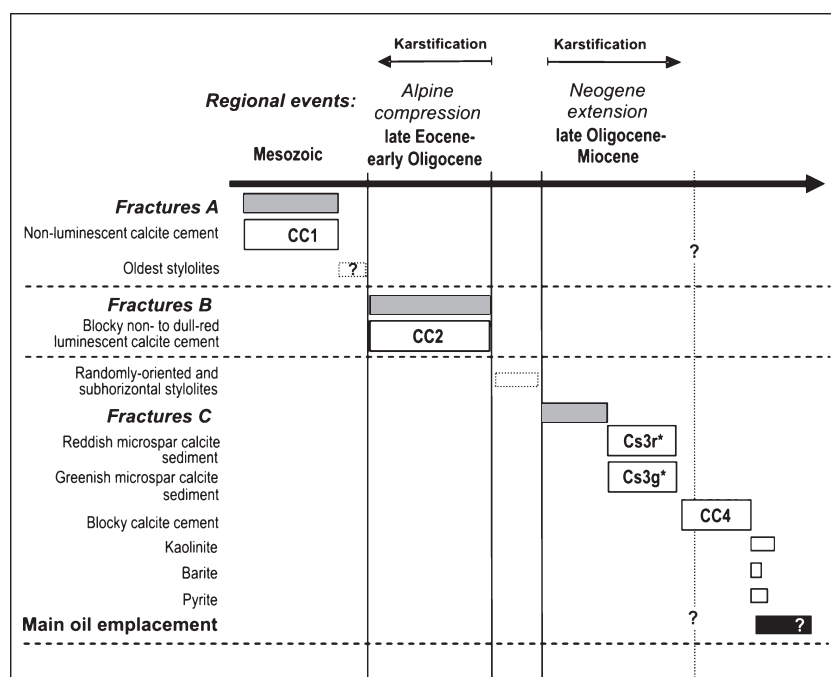

Fig. 10. Diagenetic evolution of the Amposta oil reservoir rocks and possible relationships with the main tectonic events. See legend in Table 1 for CC1, CC2, CS3 and CC4. CS3r*-CS3g*: this event includes detrital (karstic) deposition and recrystallization of CS3.
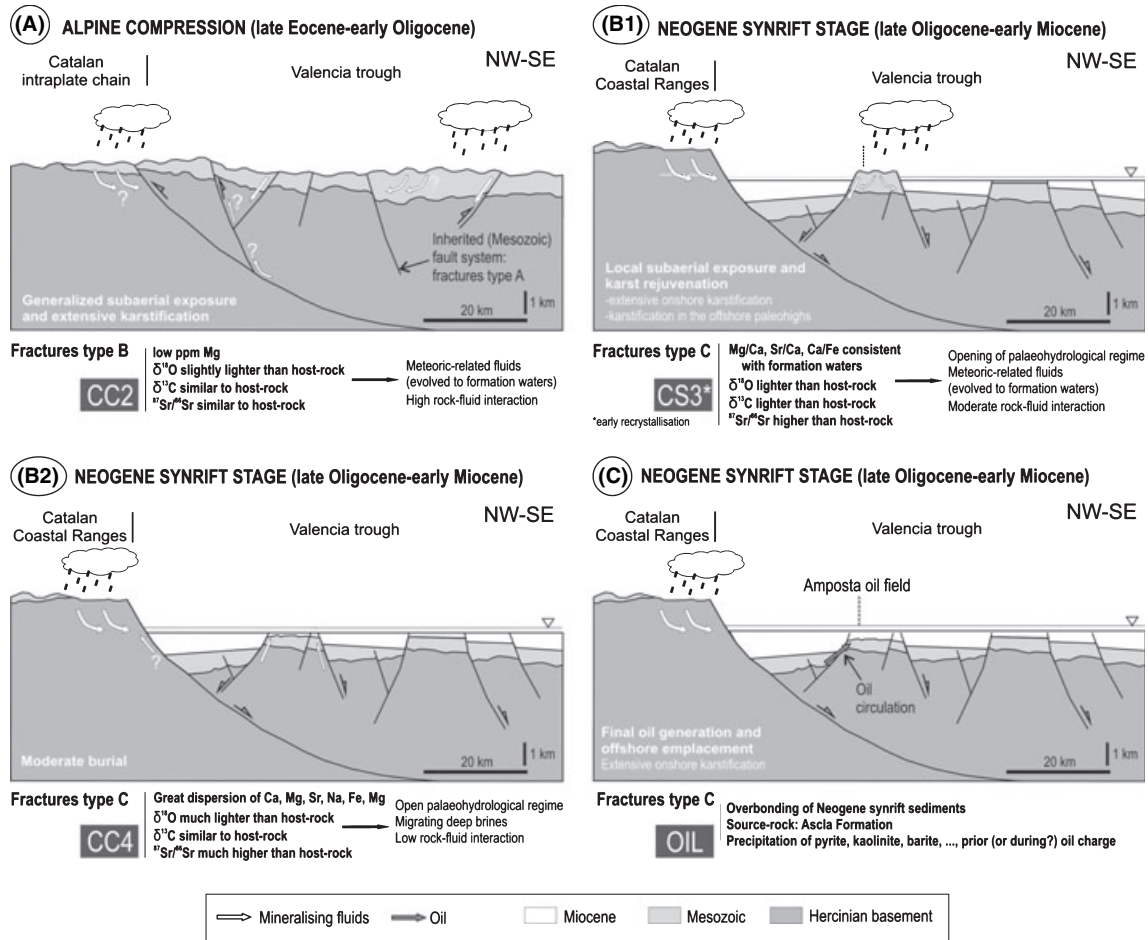
Fig. 11. Evolution of fluid migration pathways during the Palaeogene and Neogene main tectonic events.

Table 6 Calculated δ^{18}O of the precipitating fluid for each calcite cement at different temperatures (T).

Generation	Measured δ^{13}C ‰ VPDB		Measured δ^{18}O ‰ VPDB		Calculated δ^{18}O ‰ VSMOW			
	M	SD	M	SD	T = 25°C	T = 50°C	T = 95°C	T = 115°C
Marine host-limestones	+1.2	0.2	−3.2	0.6	–	–	–	–
CC2	+0.6	0.3	−7.7	1.2	**−5.7**	**+0.3**	+11.0	+15.7
CS3r	−1.7	2.4	−8.5	1.7	**−6.4**	**−0.5**	+10.3	+15.0
CS3g	−0.3	0.5	−6.6	2.5	**−4.6**	**+1.4**	+12.1	+16.8
CC4	+0.5	0.3	−12.4	0.9	−10.2	−4.3	**+6.4**	**+11.2**

See legend in Table 1 for CC1, CC2, CS3 and CC4. Bold δ^{18}O **VSMOW** values: calculated oxygen isotopic compositions of fluids for the most probable calcite precipitation temperatures.

stones, it has been suggested that direct precipitation in pore spaces occurred (Maliva *et al.* 1999; Marfil *et al.* 2003), but specific processes involving kaolinite cementation have not been geochemically and thermodynamically explained. Presence of relicts of calcite cement within the kaolinite patches in the studied samples (Fig. 9E) suggests a replacive origin for the kaolinite.

Pyrite is the second most abundant exotic mineral in the studied samples. Many sulphur bearing minerals have been described as part of the exotic mineral assemblage in carbonate reservoirs, with anhydrite being the most volumetrically-significant; precipitation of anhydrite is generally associated with occurrence of evaporite units in the basin (Neilson & Oxtoby 2008). Nevertheless, anhydrite has not been

observed in the Amposta samples. Precipitation of pyrite in type C fractures requires an external sulphur source, as either a sulphate or sulphide species. Sulphate species could be related to dissolved marine-derived sulphate, residual evaporite brines or dissolution of sulphate rocks. Evidence of seawater circulation (or residual pore-trapped seawater within the limestones) has not been observed in the whole diagenetic sequence from the Amposta rocks. Similarly, significant amount of enclosing sulphate minerals have not been encountered in the Jurassic-Cretaceous rocks of the studied area. Thick successions of evaporites occur in the underlying Triassic units; however, all effective porosity in sulphate and chloride deposits was occluded earlier, at very shallow depths (by 100 m of burial, halite units are tight and impervious; Casas & Lowenstein 1989; Warren 1999). On the other hand, the gypsum to anhydrite transformation of Triassic sulphates, which implies expulsion of large quantities of brine, most probably occurred from few metres to about one kilometre depth (Warren 2006), and therefore also much before pyrite precipitation. Thus it is unlikely that marine- or evaporite-derived sulphate was important during burial diagenesis.

Other sources of sulphur as reduced suphide (mainly H_2S) species can be invoked; main sources of reactive sulphides are thermal decomposition or organic sulphur compounds in kerogen or oil or sulphate reduction (bacterial sulphate reduction (BSR), or thermochemical sulphate reduction (TSR); Worden & Smalley 1996). Temperatures of more than 175°C are thought to be required to cause the decomposition of organic matter (Cai *et al.* 2001). Temperatures in source rocks did not exceed 111°C (Permanyer & Salas 2005), and assuming that temperatures in petroleum fluids during pyrite precipitation where from 96°C (temperature for CC4 precipitation) to 126°C (present oil field temperature; Seemann *et al.* 1990), the necessary high temperatures for this process were not attained. The Amposta crude is sulphur-rich (5–7% in weight; Seemann *et al.* 1990), but with low H_2S contents (lower than 0.2%; R. del Potro-Escal UGS, *pers. comm.*). Seemann *et al.* (1990) interpreted that this crude was expelled from a carbonate-rich source rock with high sulphur content. The Ascla Formation source rock was deposited in relatively reducing conditions favouring BSR processes (Salas & Permanyer 2003; Permanyer & Salas 2005). BSR results in a large isotopic difference between the parental sulphate and the resulting H_2S, from −25 to −50‰ (Kemp & Thode 1968; Fritz *et al.* 1989), but negligible isotopic changes seem to occur between H_2S gas and resulting sulphide minerals (Nakai & Jensen 1964). Sulphur isotopic composition of Lower Cretaceous marine-derived sulphate is around +13 or +16‰ (Claypool *et al.* 1980; Kampschulte & Strauss 2004; Paz *et al.* 2005); thus, the low $\delta^{34}S$ values of the analysed pyrites in fractures in the Amposta rocks (from −16.7‰ to −13.0‰ VCDT) are

in agreement with the expected values after BSR. Thus, expelled fluids from the petroleum source rock (Ascla Fm) are considered as being responsible for the sulphur (pyrite) contribution into the Amposta reservoir rock. On the other hand, low H_2S contents of the Amposta crude support this interpretation, rather than having been originated from thermochemical sulphate reduction (Machel *et al.* 1995; Worden & Smalley 1996; Cai *et al.* 2001; Worden *et al.* 2003). Available Fe in the Amposta rocks, possibly from dissolution of host-limestones and calcite cements during kaolinite formation under acidic conditions, partially inhibited H_2S accumulation and favoured pyrite precipitation. Cai *et al.* (2005) also interpreted H_2S accumulation due to escape of free H_2S from the source rock to the reservoir and prior to pyrite formation.

As petroleum emplacement seemingly does not entirely stop precipitation of other exotic minerals (Neilson & Oxtoby 2008), sulphur-rich fluids could circulate prior or during petroleum charge in the reservoir (Fig. 11) producing pyrite precipitation.

Oil generation and emplacement

Most oil in the Valencia Trough fields was sourced from the lower and middle Miocene organic-rich, dark brown, hemi-pelagic marls of the Alcanar Group, also named Casablanca Formation (Albaigés *et al.* 1986; Clavell & Berastegui 1991; Fig. 2). In these rocks the oil generation and migration began in the late Miocene toearly Pliocene (Clavell & Berastegui 1991; Varela *et al.* 2005).

In the adjacent onshore Maestrat basin, the Jurassic Ascla Formation has been identified as an alternative oil source rock; petroleum generation started when the Ascla shales entered the oil window at 90–100 Myr (Turonian; Permanyer & Salas 2005). Oil migration and petroleum charge in the Maestrat basin occurred during the Late Cretaceous-early Tertiary (Rossi *et al.* 2001; Salas & Permanyer 2003; Permanyer & Salas 2005), before the Alpine compressive tectonism that uplifted the onshore area promoting karstification and erosion of the potential onshore reservoirs. The Amposta oil, although being in the Valencia Trough, was sourced from the Jurassic Ascla Formation (Seemann *et al.* 1990; Salas & Permanyer 2003; Permanyer & Salas 2005; Varela *et al.* 2005; Fig. 2B), as in the neighbouring onshore Maestrat basin. Nevertheless, migration of oil from the Ascla Formation towards the Cretaceous rocks occurred necessarily after deposition of the Lower Miocene clastic sediments that seal the reservoir (Fig. 3) and, therefore, later than in the Maestrat onshore basin.

Burial and thermal model of the Marino C3 well (location in Fig. 1) suggested two-stage oil generation from the Ascla marls in the Amposta reservoir (Permanyer & Salas 2005): i) a first stage during the late Cretaceous to early Tertiary, analogous to that in the onshore setting, and, ii) a second

stage of generation when the Ascla Formation was at, or close to, the maximum burial depth, induced by the overburden Neogene synrift sediments, during the Miocene. The diagenetic sequence observed in the present work on the well Amposta Marino C-2 indicates that the main oil emplacement took place after precipitation of CC4, probably during a late stage of the Neogene extensional regime (Fig. 10).

Oil circulation in the Amposta reservoir occurred in partially uncemented fractures, open stylolites, the intercrystalline porosity and apparently along the cleavage planes of the CC4 crystals. Esteban & Taberner (2003) proposed a paragenetic scheme that concurs with the observations reported here of burial-related corrosion of CC4 prior to (or during) oil migration. These authors compiled data from productive carbonate rocks from different geologic provinces and concluded that major and minor corrosion stages (and porosity generation) occurred during burial diagenesis of carbonate reservoirs, leading or preceding the roll-front of petroleum migration. However, the studied samples from Amposta Marino C2 well do not provide clear evidence of major porosity enhancement in burial conditions, thus suggesting that major secondary porosity was produced instead by meteoric diagenesis (Orlopp 1988; Seemann et al. 1990; Clavell & Berastegui 1991).

The original oil water contact (OWC) in the Amposta oil field was at 1940 m TVD below sea level (data obtained in 1970 in the Amposta discovery well; Seemann et al. 1990; Fig. 3). Petrographical observations in the Amposta Marino C-2 well are in accordance with the OWC; the remaining porosity and macroscopic oil impregnation occur in the rocks above 1910.8 sample (Table 1), while the original porosity is nearly totally obliterated by cementation in the limestones below 1943.5 metres (there are no available data between these samples).

CONCLUSIONS

The main oil migration in the Amposta oil reservoir is related in time to Neogene extensional fractures. Three fracturing stages have been identified in the Barremian–Aptian reservoir rocks of the Amposta field. Fracture types A and B are attributed to early fractures developed prior to, and during the Alpine compression and are totally filled by calcite cement 1 (CC1) and 2 (CC2), respectively. Fracture type C developed during Neogene extension, and is filled by reddish and greenish microspar calcite sediment (CS3r and CS3g), blocky calcite cement 4 (CC4), kaolinite, pyrite, barite and oil.

The entire diagenetic sequence indicates a closed palaeohydrological system and a high degree of fluid-rock interaction during precipitation of CC2 (Alpine compression). During the Tertiary extension, the system became open to more radiogenic external fluids. Type C fractures were enlarged by subaerial exposure. Evolved-meteoric

waters were responsible of CS3 recrystallization, after sedimentation of detrital CS3 in the karstic terrain. Progressive re-burial was recorded by precipitation of CC4 as a result of migration of hot and $\delta^{18}O$-enriched brines.

The main oil migration postdates CC4 precipitation. Oil circulated through partially cemented fractures, open stylolites, intercrystalline porosity and in the cleavage planes of the CC4 crystals. Burial dissolution of CC4 occurred prior to, or during, oil charge, possibly related to kaolinite precipitation (i.e. acid fluids). The sulphur source associated with the late precipitation of pyrite was likely related to isotopically-light sulphur expelled, e.g. as sulphide, from the petroleum source rock (Ascla Fm).

REFERENCES

Albaigés J, Algaba J, Clavell E, Grimalt J (1986) Petroleum geochemistry of the Tarragona Basin (Spanish mediterranean offshore). *Organic Geochemistry*, **10**, 441–50.

Banner JL, Hanson GN (1990) Calculations of simultaneous isotopic and trace element variations during water-rock interaction with applications to carbonate diagenesis. *Geochimica et Cosmochimica Acta*, **54**, 3123–37.

Burke WH, Denison RE, Hetherington EA, Koepnick RB, Nelson HF, Otto JB (1982) Variation of seawater $^{87}Sr/^{86}Sr$ throughout Phanerozoic time. *Geology*, **10**, 516–9.

Burton EA, Walter LM (1991) The effects of P_{CO_2} and temperature on magnesium incorporation in calcite in seawater and $MgCl_2$-$CaCl_2$ solutions. *Geochimica et Cosmochimica Acta*, **55**, 777–85.

Cai C, Hu W, Worden RH (2001) Thermochemical sulphate reduction in Cambro-Ordovician carbonates in Central Tarim. *Marine and Petroleum Geology*, **18**, 729–41.

Cai C, Worden RH, Wolff GA, Bottrell SH, Wang D, Li X (2005) Origin of sulphur rich oils and H_2S in Tertiary lacustrine

sections of the Jinxiang Sag, Bohai Bay Basin, China. *Applied Geochemistry*, **20**, 1427–44.

Calvet F, Permanyer A, Vaquer R (1983) El paleokarst del contacto Mesozoico-Mioceno en el Penedés y Camp de Tarragona. *X Congreso Español de Sedimentología*. Menorca, 173–175, communication.

Casas E, Lowenstein TK (1989) Diagenesis of saline pan halite; comparison of petrographic features of modern, Quaternary and Permian halites. *Journal of Sedimentary Petrology*, **59**, 724–39.

Clavell E, Berastegui X (1991) Petroleoum geology of the Gulf of València. In: *Generation, Accumulation, and Production of Europe's Hydrocarbons* (ed. Spencer MA), pp. 355–68. Oxford University Press, Oxford. Special Publication of the European Association of Petroleoum Geoscientists, **1**.

Claypool GE, Holser WT, Kaplan YR, Sakai H, Zak I (1980) The age of sulfur and oxygen isotopes in marine sulfate and their mutual interpretation. *Chemical Geology*, **28**, 199–260.

Craig H (1965) The measurement of oxygen isotope paleotemperatures. In: *Stable Isotopes in Oceanographic Studies and Paleotemperatures* (ed Tongiorgi E), pp. 161–82. Consiglio Nazionale delle Ricerche, Laboratario di Geologia Nucleare, Pisa.

Dromgoole EL, Walter LM (1990) Iron and manganese incorporation into calcite: effects of growth kinetics, temperature and solution chemistry. *Chemical Geology*, **81**, 311–36.

Esteban M (1973) *Petrología de las Calizas Cretácicas del Sector Central de los Catalánides (Prov. de Tarragona y Barcelona)*. PhD Thesis, Universitat de Barcelona, Barcelona, unpublished.

Esteban M (1991) Palaeokarst: case histories. In: *Palaeokarsts and Palaeokarstic Reservoirs* (eds Wright VP, Esteban M, Smart PL), pp. 120–46. Postgraduate Research Institute for Sedimentology, University of Reading, Reading. 152.

Esteban M, Julià R (1973) Discordancias erosivas intrajurásicas en los Catalánides. *Acta Geológica Hispánica*, **8**, 153–7.

Esteban M, Klappa CF (1983) Subaerial Exposure Environment. In: *Carbonate Depositional Environments* (eds. Scholle PA, Bebout DG, Moore CH), pp. 2–54. American Association of Petroleum Geologists, Tulsa. **33**.

Esteban N, Taberner C (2003) Secondary porosity development during late burial in carbonate reservoirs as a result of mixing and/or cooling of brines. *Journal of Geochemical Exploration*, **78-79**, 355–9.

Fritz P, Basharnal GM, Drimmie RJ, Ibsen J, Qureshi RM (1989) Oxygen isotope exchange between sulphate and water during bacterial reduction of sulphate. *Chemical Geology*, **79**, 99–105.

Gaspar-Escribano JM, García-Castellanos D, Roca E, Cloetingh S (2004) Cenozoic vertical motions of the Catalan Coastal Ranges (NE Spain): The role of tectonics, isostasy, and surface transport. *Tectonics*, **23**, TC1004. doi: 10.1029/2003TC001511.

Grötsch J, Vahrenkamp V (1995) Can carbon isotopes be used as a stratigraphic tool in Mid-Cretaceous shallow water carbonates? *AAPG Bulletin*, **79**, 1218.

Hardenbol J, Thierry J, Farley MB, Jacquin T, Graciansky PC, Vail PR (1998) Mesozoic and Cenozoic Sequence Chronostratigraphic Framework of European basins (Cretaceous Biochronostratigraphy, Chart 5). In: *Mesozoic and Cenozoic Sequence Stratigraphy of European Basins* (eds. De Graciansky PC, Hardenbol J, Jacquin Th, Vail PR)), pp. 3–13. SEPM Special Publication 60, Tulsa.

Howson MR, Pethybridge AD, House WA (1987) Synthesis and distribution coefficient of low-magnesium calcites. *Chemical Geology*, **64**, 79–87.

Jenkyns HC, Jones CE, Gröcke DR, Hesselbo SP, Parkinson DN (2002) Chemostratigraphy of the Jurassic System: applications,

limitations and implications for palaeoceanography. *Journal of Geological Society of London*, **159**, 351–78.

Jones CE, Jenkyns HC, Coe AL, Hesselbo SP (1994) Strontium isotope variations in Jurassic and Cretaceous seawater. *Geochimica et Cosmochimica Acta*, **58**, 3061–74.

Kampschulte A, Strauss H (2004) The sulphur isotopic evolution of Phanerozoic seawater based on the analysis of structurally substituted sulfate in carbonates. *Chemical Geology*, **204**, 255–86.

Katz A (1973) The interaction of magnesium with calcite during crystal growth at 25-90°C and one atmosphere. *Geochimica et Cosmochimica Acta*, **37**, 1563–86.

Katz A, Sass E, Starinsky A, Holland HD (1972) Strontium behavior in the aragonite-calcite transformation: An experimental study at 40–98°C. *Geochimica et Cosmochimica Acta*, **36**, 481–96.

Kemp AL, Thode HG (1968) The mechanism of the bacterial reduction of sulphate and of sulphite from isotope fractionation studies. *Geochimicat et Cosmochimica Acta*, **32**, 71–91.

Kinsman DJJ (1969) Interpretation of Sr^{+2} concentrations in carbonate minerals and rocks. *Journal of Sedimentary Petrology*, **39**, 486–508.

Klimowitz J, Hernández E, Serrano A (2005) A field trip guide book. The Mediterranean Basin (Catalan costal range onshore analogues). In: *Asociación de Geólogos y Geofísicos Españoles del Petróleo (AGGEP)-XXV Aniversario* (ed. Martínez del Olmo W), 187–208. Museo de Ciencias Naturales, Madrid.

Koepnick RB, Burke WH, Denison RE, Hetherington EA, Nelson HF, Otto JB, Waite LE (1985) Construction of the seawater $^{87}Sr/^{86}Sr$ curve for the Cenozoic and Cretaceous: supporting data. *Chemical Geology*, **58**, 55–81.

Kupecz JA, Land LS (1994) Progressive recrystallization and stabilization of early-stage dolomite: lower Ordovician Ellenburger Group, West Texas. *Special Publication of the International Association of Sedimentologists*, **21**, 255–79.

Lawrence SR, Cornford C (1995) Basin geofluids. *Basin Research*, **7**, 1–7.

Lomando AJ, Harris PM, Orlopp DE (1993) Casablanca field, Tarragona Basin, offshore Spain: a karsted carbonate reservoir. In: *Paleokarst Related Hydrocarbon Reservoirs* (eds. Fritz RD, Wilson JL, Yurewicz DA) Core Workshop, 18, in New Orleans, SEPM 201–25, Tulsa.

Losantos M, Aragonès E, Berástegui X, Palau J, Puigdefàbregues C (1989) *Mapa Geològic de Catalunya*, scale 1:25000. Servei Geològic de Catalunya, Barcelona.

Machel HG, Krouse HR, Sassen R (1995) Products and distinguishing criteria of bacterial and thermochemical sulfate reduction. *Applied Geochemistry*, **10**, 373–89.

Maliva RG, Dickson JAD, Fallick AE (1999) Kaolin cements in limestones: potential indicators of organic-rich pore waters during diagenesis. *Journal of Sedimentary Research*, **69**, 158–63.

Malone MJ, Baker PA, Burns SJ (1994) Recrystallization of dolomite: evidence from the Monterey Formation (Miocene) California. *Sedimentology*, **41**, 1223–39.

Marfil R, Delgado A, Rossi C, La Iglesia A, Ramseyer K (2003) Origin and diagenetic evolution of kaolin in reservoir sandstones ans associated shales of the Jurassic and Cretaceous, Salam Field, Western Desert (Egypt). *IAS Special Publication*, **34**, 319–42.

Marfil R, Caja MA, Tsige M, Al-Aasm IS, Martín-Crespo T, Salas R (2005) Carbonate-cemented stylolites and fractures in the Upper Jurassic limestones of the Eastern Iberian Range, Spain:

A record of palaeofluids composition and thermal history. *Sedimentary Geology*, **178**, 237–57.

Marshall JD (1992) Climatic and oceanographic isotopic signals from the carbonate rock record and their preservation. *Geological Magazine*, **129**, 143–60.

Martinez del Olmo W, Esteban M (1983) Paleokart Development. In: *Carbonate Depositional Environments* (eds. Scholle PA, Bebout DG, Moore CH) *American Association of Petroleum Geologists*, **33**, 93–5. AAPG, Tulsa.

McIntire WL (1963) Trace element partition coefficients — a review of theory and applications to geology. *Geochimica et Cosmochimica Acta*, **27**, 1209–64.

Merten R (2006) Petroleum exploration and production in Spain. In: *Contributions to the Geology of Spain* (eds. Schroeder R, Perejón A) *Zeitschrift der Deutschen Gesellschaft für Geowissenschaften*. **157/4**, 717–32. Verlagsbuchhandlung, Stuttgart.

Meyers WJ, Lohmann KC (1985) Isotope geochemistry of regionally extensive calcite cement zones and marine components in Mississippian limestones, New Mexico. In: *Carbonate Cements* (eds. Schneidermann N, Harris PM). *SEPM Special Publication*, **36**, 223–39.

Montañez IP (1994) Late diagenetic dolomitization of Lower Ordovician, Upper Knox Carbonates: a record of the hydrodynamic evolution of the southern Appalachian Basin. *AAPG Bulletin*, **78**, 1210–39.

Mucci A (1987) Influence of temperature on the composition of magnesian calcite overgrowths precipitated from seawater. *Geochimica et Cosmochimica Acta*, **51**, 1977–84.

Mucci A, Morse JW (1983) The incorporation of Mg^{2+} and Sr^{2+} into calcite overgrowths: influences of growth rate and solution composition. *Geochimica et Cosmochimica Acta*, **47**, 217–33.

Nakai N, Jensen ML (1964) The kinetic isotope effect in the bacterial reduction and oxidation of sulfur. *Geochimicat et Cosmochimica Acta*, **28**, 1893–912.

Neilson JE, Oxtoby NH (2008) The relationship between petroleum, exotic cements and reservoir quality in carbonates – a review. *Marine and Petroleum Geology*, **25**, 778–90.

Orlopp DE (1988) Casablanca oil field, Spain: a karsted Carbonate trap at the shelf edge. *Proceedings of the Offshore Technology Conference*, OTC Publisher (Offshore Technology Conference), Houston.

Paquette J, Reeder RJ (1995) Relationship between surface structure, growth mechanism, and trace element incorporation in calcite. *Geochimica et Cosmochimica Acta*, **59**, 735–49.

Paz JDS, Rossetti DF, Macambira MJB (2005) An Upper Aptian saline pan/lake system from the Brazilian equatorial margin: integration of facies and isotopes. *Sedimentology*, **52**, 1303–21.

Permanyer A, Salas R (2005) Integrated thermal model, diagenetic history and oil correlation in western Mediterranean, Spain. *IV ALAGO Workshop on Basin Modeling*, Buenos Aires, Communication.

Pirrie D, Marshall JD (1990) High-paleolatitude Late Cretaceous paleotemperatures: new data from James Ross Island, Antarctica. *Geology*, **18**, 31–4.

Reeder RJ, Grams JC (1987) Sector zoning in calcite cement crystals: implications for trace element distributions in carbonates. *Geochimica et Cosmochimica Acta*, **51**, 187–94.

Reinhold C (1998) Multiple episodes of dolomitization and dolomite recrystallization during shallow burial in Upper Jurassic shelf carbonates; eastern Swabian Alb, southern Germany. *Sedimentary Geology*, **121**, 71–95.

Roca E, Sans L, Cabrera L, Marzo M (1999) Oligocene to middle Miocene evolution of the central Catalan margin (northwestern Mediterranean). *Tectonophysics*, **315**, 209–29.

Rossi C, Goldstein RH, Marfil R, Salas R, Benito MI, Permanyer A, de la Peña JA, Caja MA (2001) Diagenetic and oil migration of the Kimmeridgian Ascla formation, Maestrat Basin, Spain. *Marine and Petroleum Geology*, **18**, 287–306.

Salas R, Casas A (1993) Mesozoic extensional tectonics, stratigraphy, and crustal evolution during the Alpine cycle of the eastern Iberian basin. *Tectonophysics*, **228**, 33–55.

Salas R, Permanyer A (2003) Evidencias de generación de hidrocarburos en la formación de margas del Mas d'Ascla (Jurásico superior, Cadena Ibérica oriental) y su relación con el campo de Amposta de la Cuenca de Tarragona. *Boletín Geológico y Minero*, **114**, 75–86.

Salas R, Guimerà J, Mas R, Martín-Closas C, Meléndez A, Alonso A (2001) Evolution of the Mesozoic Central Iberian Rift System and its Cainozoic inversion (Iberian Chain). In: *Peri-Tethys Memoir 6: Per-Tethyan Rift/Wrench Basins and Passive Margins* (eds. Ziegles PA, Cavazza W, Robertson AHF & Crasquin-Soleau S) *Mémoires du Museum National d'Histoire Naturelle*, **186**, 145–85. Muséum National d'Histoire Naturelle, Paris.

Salas J, Taberner C, Esteban M, Ayora C (2007) Hydrothermal dolomitization, mixing corrosion and deep burial porosity formation: numerical results from 1-D reactive transport model. *Geofluids*, **7**, 99–111.

Seemann U, Pümpin VF, Casson VF (1990) Amposta oil field. *AAPG Treatise of Petroleum Geology, Atlas of oil and gas fields*, **A-017**, 1–20.

Skougstad MW, Horr CA (1963) Occurrence and distribution of strontium in natural waters. *US Geological Survey Water Supply Paper*, **1496-D**, 55–97.

Stoessell RK, Klimentidis RE, Prezbindowski DR (1987) Dedolomitization in Na–Ca–Cl brines from 100° to 200°C at 300 bars. *Geochimica et Cosmochimica Acta*, **51**, 847–55.

Travé A, Calvet F (2001) Syn-rift geofluids in fractures related to th early-middle Miocene evolution of the Vallès-Penedès halfgraben (NE Spain). *Tectonophysics*, **336**, 101–20.

Travé A, Calvet F, Soler A, Labaume P (1998) Fracturing and fluid migration during Palaeogene compression and Neogene extension in the Catalan Coastal Ranges, Spain. *Sedimentology*, **45**, 1063–82.

Tucker ME, Wright VP (1990) *Carbonate Sedimentology*. Blackwell Scientific Publications, Oxford.

Varela J, Vicente-Bravo JC, Navarro J, Esteban M, Martínez del Olmo W (2005)The oil fields in the Spanish Mediterranean Sea. In: *Asociación de Geólogos y Geofísicos Españoles del Petróleo (AGGEP)-XXV Aniversario* (ed. Martínez del Olmo W), 121–30. Museo de Ciencias Naturales, Madrid.

Vegas R, de Vicente G (2004) El surco de Valencia. In: *Geología de España* (ed. Vera JA) p. 615. Sociedad Geológica de España-Instituto Geológico y Minero de España, Madrid.

Veizer J, Compston W (1974) $^{87}Sr/^{86}Sr$ composition of seawater during the Phanerozoic. *Geochimica et Cosmochimica Acta*, **38**, 1460–84.

Veizer J, Hoefs J (1976) The nature of O^{18}/O^{16} and C^{13}/C^{12} secular trends in sedimentary carbonate rocks. *Geochimica et Cosmochimica Acta*, **40**, 1387–95.

Veizer J, Buhl D, Diener A, Ebneth S, Podlaha OG, Bruckschen P, Jasper T, Korte C, Schaaf M, Ala D, Azmy K (1997) Strontium isotope stratigraphy: potential resolution and event correlation. *Palaeogeography, Palaeoclimatology, Palaeoecology*, **132**, 65–77.

Warren J (1999) *Evaporites. Their Evolution and Economics.* Blackwell Science, Great Britain.

Warren J (2006) *Evaporites. Sediments, Resources and Hydrocarbons.* Springer, Germany.

Watson HJ (1982) Casablanca field offshore, a paleogeomorphic trap. In: The Deliberate Search for the Subtle Trap, *AAPG Memoir*, **32**, 237–50.

Worden RH, Smalley PC (1996) H_2S-producing reactions in deep carbonate gas reservoirs: khuff formation, Abu Dhabi. *Chemical Geology*, **133**, 157–71.

Worden RH, Smalley PC, Barclay SA (2003) H_2S and diagenetic pyrite in North Sea sandstones: due to TSR or organic sulphur compound cracking? *Journal of Geochemical Exploration*, **78-79**, 487–91.